Parametric Investigation of the Effect of Hub Pitching Moment on Blade Vortex Interaction (BVI) Noise of an Isolated Rotor

Carlos Malpica
Aerospace Engineer
NASA Ames Research Center
Moffett Field, CA

Eric Greenwood
Aerospace Engineer
NASA Langley Research Center
Hampton, VA

Ben Sim
Research Engineer
US Army Aviation Development Directorate
Moffett Field, CA

ABSTRACT

At the most fundamental level, main rotor loading noise is caused by the harmonically-varying aerodynamic loads (acoustic pressures) exerted by the rotating blades on the air. Rotorcraft main rotor noise is therefore, in principle, a function of rotor control inputs, and thus the forces and moments required to achieve steady, or "trim", flight equilibrium. In certain flight conditions, the ensuing aerodynamic loading on the rotor(s) can result in highly obtrusive harmonic noise. The effect of the propulsive force, or *X*-force, on Blade-Vortex Interaction (BVI) noise is well documented. This paper presents an acoustics parametric sensitivity analysis of the effect of varying rotor aerodynamic pitch hub trim moments on BVI noise radiated by an S-70 helicopter main rotor. Results show that changing the hub pitching moment for an isolated rotor, trimmed in nominal 80 knot, 6 and 12 deg descent, flight conditions, alters the miss distance between the blades and the vortex in ways that have varied and noticeable effects on the BVI radiated-noise directionality. Peak BVI noise level is however not significantly altered. The application of hub pitching moment allows the attitude of the fuselage to be controlled; for example, to compensate for the uncomfortable change in fuselage pitch attitude introduced by a fuselage-mounted *X*-force controller.

NOMENCLATURE

C_{M_x}	rolling moment coefficient
C_{M_y}	pitching moment coefficient
C_T	thrust coefficient
M_y	pitching moment, ft-lb
R	rotor radius, ft
V_∞	velocity, ft/s
α_{TPP}	tip path plane angle of attack, deg
β_{1c}	longitudinal blade flapping, deg
β_{1s}	lateral blade flapping, deg
γ	flight path angle, deg
θ_s	rotor shaft angle, deg
σ	rotor solidity
Ω	rotor rotational speed, rad/s

INTRODUCTION

Background

The high levels of noise generated by helicopter operations remain at the heart of public opposition to the widespread use of helicopters for commercial transportation. Harmonic rotor noise is a major contributor to the noise generated by helicopters. There are multiple mechanisms that generate harmonic rotor noise (Ref. 1). Conventionally, main rotor harmonic noise has been taken to be a function of four governing parameters, i.e., advancing tip Mach, advance ratio, thrust coefficient, and tip-path-plane (TPP) angle of attack.

Blade-Vortex Interaction (BVI) is well known to be a significant source of rotor harmonic noise that extends to high frequencies. BVI noise originates from the sharp acoustic pulses that result from a rotor blade passing in close proximity to, or even striking, a blade tip vortex from the wake. The advancing tip Mach number and advance ratio are assumed to control the "top-view" geometry of the rotor wake, shown in Figure 1, defining the number, location and interaction angles of the BVI across the rotor disk. The thrust coefficient and tip-path-plane angle of attack are assumed to define the longitudinal trim of the helicopter and determine the inflow through the rotor disk. These parameters therefore control the "side-view" geometry of the wake, shown in Figure 2, setting the "miss distance" between the wake vortices and the rotor blades at each interaction location. The intensity of the BVI is strongly dependent on this miss distance. The thrust coefficient also controls the circulation strength of the vortices at their time of release from the leading edge of the rotor disk, with a corresponding influence on the intensity of BVI noise.

BVI noise is a problem for civilian helicopter terminal area operations because it manifests itself in descending flight, where BVI miss distances are low, with the peak BVI noise levels occurring near the standard 6-9 degree approach glide path angles (GPA). The intermittent nature of BVI

Presented at the AHS 72nd Annual Forum, West Palm Beach, Florida, USA, May 17-19, 2016.

noise is arguably an annoyance, which tends to draw attention to the helicopter (Ref. 2).

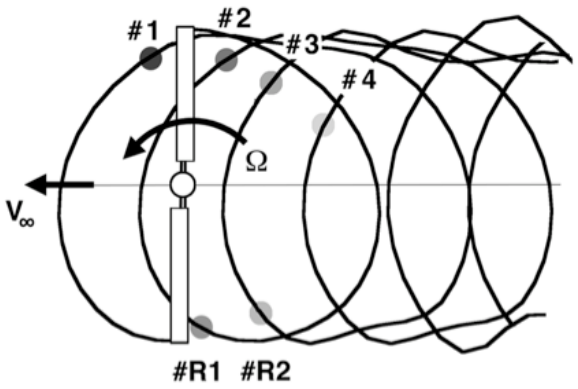

Figure 1. "Top-view" wake geometry for a two-bladed rotor. (Ref. 1)

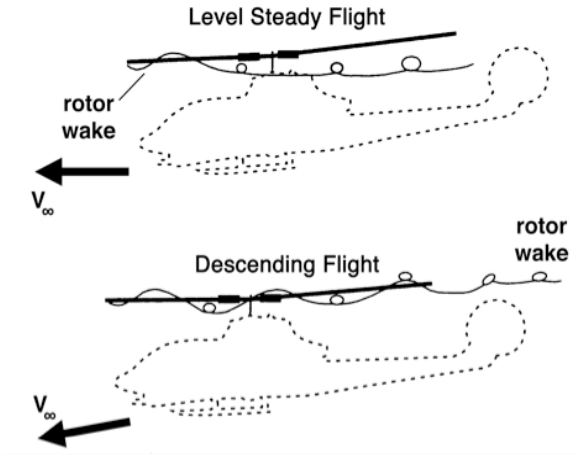

Figure 2. "Side-view" wake geometry. (Ref. 1)

Existing rotor noise attenuation techniques all operate under the same fundamental principle: to suppress the noise source, i.e., the impulsive aerodynamic forces on the blades. Techniques include careful management or control of the approach flight path, flow control on the blade, custom tip shapes, and active rotor control systems. Active rotor control, such as Individual Blade Control (IBC) using blade root-actuated systems in Ref. 3 and active flaps in the case of Ref. 4, operates by directly affecting the blade loading. These approaches have been shown to be effective in reducing both BVI and low frequency noise.

Alternatively, BVI noise can be attenuated by modifying the trim state of the rotor, primarily altering the tip-path-plane angle of attack and wake geometry. One such technique is proposed in Ref. 5, where by varying the propulsive requirement on the rotor in trim (the *X*-force), the rotor plane must tilt proportionately in order to maintain vehicle equilibrium. This basic principle was also at the heart of the research of Ref. 6, which showed that flying decelerating approaches could affect BVI noise by altering the rotor tip-path-plane angle of attack and wake geometry. The same fundamental principles have also been successfully analyzed on the XV-15 tiltrotor in Ref. 7.

The effect of airframe drag effectors on BVI noise radiation of a helicopter in trim was revisited in Ref. 8 for an S-70 helicopter (Figure 3). Introducing airframe drag (*X*-force) ideally at the center-of-gravity causes the rotor tip-path-plane to tilt more nose-down to generate enough propulsive force for vehicle trim. That study confirmed that the primary mechanism for BVI noise reduction was achieved through the reorientation of the tip-path plane angle of attack that increases BVI miss distance by displacing the wake further away from the rotor (Figure 3b). However, it was also noted in Ref. 8 that introducing an *X*-force tends to result in a nose-down fuselage pitch angle not favored by pilots. Reference 8 further suggested that if the *X*-force is offset from the C.G. (Figure 3c), it is possible to recover the fuselage pitch angle to a more favorable state, without compromising the benefits of reduced BVI noise. However, this implies that the rotor hub must carry additional hub pitching moments to maintain vehicle trim. To-date, the effects of hub pitching moments on BVI noise is not well understood because of the coupled nature of longitudinal force *X* and pitching moment M_y in full-vehicle free-flight trim simulations. The hub pitching and rolling

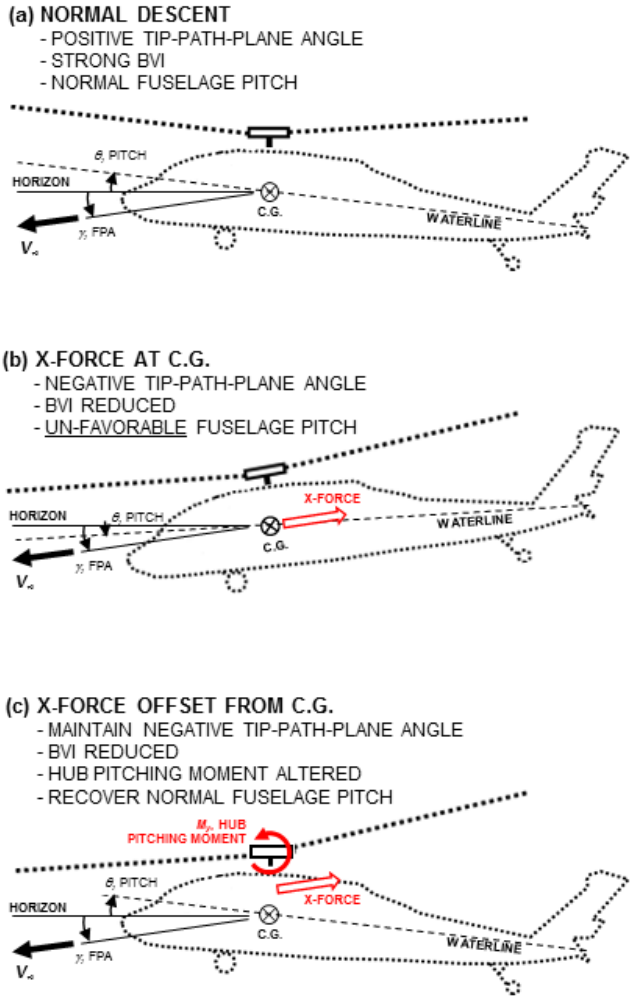

Figure 3. Effects of additional forces and moments on longitudinal trim

moments are likely to influence the rotor blade motion and airloads, and therefore constitute two parameters which might influence rotor harmonic noise radiation, in addition to the four parameters that are conventionally assumed to govern rotor harmonic noise radiation.

Objective

The aim of this study is to investigate the sensitivity of BVI noise radiation to changes in the hub pitch moment trim state, for an isolated, medium-lift helicopter main rotor under constant thrust and propulsion settings.

METHODOLOGY

Technical Approach

A parametric analysis, via sweeps of the hub pitching moment of an isolated main rotor in trim, was conducted to delineate their cause-and-effect on BVI noise. The parametric variation of the hub moment in trim was conducted under constant thrust and propulsion settings, highlighting the non-unique trim states of the rotor.

Analysis of the subject rotor was performed with the comprehensive rotorcraft aeromechanics analysis tool CAMRAD II (Ref. 9), which was used to solve for the rotor trim state, including the integrated aerodynamic loads on the blade and blade geometry. Acoustics predictions were performed primarily using the PSU-WOPWOP acoustics analysis code (Ref. 10). Procedurally, the rotor model pitch trim moment requirement parameters were varied independently while keeping rotor thrust and propulsive force (drag) requirements invariant. Trim controls were the collective, cyclic (lateral and longitudinal) and shaft pitch inputs.

The S-70 helicopter main rotor (see Table 1) was chosen in this study for consistency with the study of Ref. 8, allowing for cross-comparison of results. Incidentally, this choice offered a convenient source of aerodynamic and acoustic data measurements for model validation because instrumented UH-60/S-70 rotors have been the subject of numerous wind-tunnel and flight tests conducted by NASA and the US Army

Analysis Tools

The methodology for deriving the rotor noise predictions consisted of a one-way coupling of the comprehensive rotor analysis CAMRAD II and the acoustics analysis tool PSU-WOPWOP. CAMRAD II was used to calculate rotor blade geometry and predicted blade airloads. The latter were then used in PSU-WOPWOP to compute acoustic pressures over a specified surface in space. CAMRAD II models the blade structural properties, rotor wake geometry, and local unsteady blade aerodynamics. Within CAMRAD II, blade modeling is based on a series of span-wise distributed nonlinear beam finite elements. Each beam element is represented by a full range of blade motions, which includes axial, lead-lag, flapping and torsion. Specifically, the elastic deformation of the blade is characterized by the spatial displacements of any arbitrary point on the elastic axis and the Euler angle rotations of the blade cross-sections relative to a rotating blade frame of reference.

A non-uniform inflow model coupled to a free wake was used to obtain aerodynamic forces and blade motion solutions that satisfy the rotor thrust, propulsive force and pitch/roll moments required for the trim conditions. In all ensuing calculations, the rotor blade was modeled using twenty aerodynamic panels on each blade. The panels were more densely distributed near the tip of the rotor blade, the dominant region important for sound radiation. Steady airloads were computed using C81 airfoil tables. Unsteady lift and moment in the attached flow were calculated based on compressible thin-airfoil theory. For vehicle trim calculations the aerodynamic loads on the blades were evaluated at azimuth intervals of 15 deg. The relatively large time (azimuth) step is adequate for capturing low frequency sound, but BVI noise calculation requires a time (azimuth) step of 1 deg or smaller, to capture higher frequency content. An azimuthal resolution of 1 deg was used in this study. CAMRAD II generates this fine azimuthal resolution after achieving a converged trim solution, by reconstructing the wake geometry and blade motion at the intermediate azimuths.

CAMRAD II is capable of computing both wind-tunnel trim and free-flight, or propulsive, trim solutions. Two baseline operating conditions were defined for this study, chosen to be representative of two distinct BVI helicopter conditions: 1) a standard approach (6-deg descent angle), and 2) a steep approach (12-deg descent angle). In the context of CAMRAD II's wind-tunnel trim procedure, the shaft pitch angles for these two baseline conditions were set to match the orientation relative to the wind that would be experienced in these flight conditions.

Procedurally, the baseline wind-tunnel trim cases corresponding to the 6- and 12-deg descent conditions were evaluated in free-flight first. Shaft orientation (pitch), main rotor drag (in wind axes), thrust (in shaft axes) and hub pitching moment (in shaft axes) were then "recorded" and used to define the trim targets for the wind-tunnel trim procedure. The methodology for trimming the lateral roll moment was somewhat more liberal. For the 6-deg descent case, lateral flapping was set to satisfy the $\beta_{1s} = 0$ condition. For the 12-deg descent case, the trim problem was defined to satisfy a constant roll moment value (−930 ft-lb) to match the roll moment obtained from the free-flight solution. In all cases swashplate control inputs and rotor elastic flapping, as well as tip-path-plane angle of attack, were verified to match the free-flight trim solution.

The free-flight helicopter configuration used to define the wind-tunnel trim configurations was based on that used in Ref. 8, with 18,500 lb gross weight, at 80 knots airspeed, and −6 and −12 deg flight path angles. Results from the free-flight trim solution for the baseline cases indicated main rotor thrust and drag requirements to be:

1. $\dfrac{C_T}{\sigma} = \begin{cases} 0.080 & \text{for 6 deg descent} \\ 0.076 & \text{for 12 deg descent} \end{cases}$ (in shaft axes)

2. $\dfrac{C_X}{\sigma} = \begin{cases} 0.0046 & \text{for 6 deg descent} \\ 0.0125 & \text{for 12 deg descent} \end{cases}$ (in wind axes)

The baseline hub pitch moments were determined to be approximately in the order of −16,000 ft-lb for the 6 deg descent, and −16,600 ft-lb for the 12 deg descent. Therefore, in coefficient form:

$$\frac{C_{M_y}}{\sigma} = \begin{cases} -0.00264 & \text{for 6 deg descent} \\ -0.00274 & \text{for 12 deg descent} \end{cases}$$

The acoustics prediction code, PSU-WOPWOP, uses the blade planform, airfoil geometry, and pre-determined aerodynamic loading to resolve rotor acoustics radiation in the time-domain, based on Farassat's Formulation 1A (Ref. 11). The noise is computed for any observer in both the near- and the far-field. For this study, PSU-WOPWOP was specifically configured to use the CAMRAD II computed blade motion and unsteady airloads.

A hemispherical observer grid, similar to that used in Ref. 8, was configured for the calculation of acoustic pressures. This grid was centered at the rotor hub and aligned with the inertial (or wind-tunnel) frame of reference. Observers were placed at azimuthal intervals of 20 deg and elevation intervals of 12.5 deg starting from the horizon down to 75 deg. One additional observer was placed directly below the hub. The radial distance of the observers from the hub was 500 ft (18.63*R*). The shaft was appropriately oriented relative to the wind

The BVI Sound Pressure Level (BVI SPL) metric is used throughout this paper to characterize the BVI noise. BVI SPL was calculated in PSU-WOPWOP by integrating the sound pressure power spectra between the 10th and 50th blade passage harmonics. For a nominal rotor speed of 27 rad/s, these band-pass filter frequencies corresponded to approximately 172 and 860 Hz, respectively.

Rotor Configuration and Atmospheric Conditions

The CAMRAD II S-70/UH-60 main rotor model used was the same as in Ref. 8. The model consisted of the single main rotor only. The rotor was isolated, so all aerodynamic interferences were omitted. Main rotor characteristics and atmospheric flow conditions are summarized in Tables 1 and 2, respectively.

Table 1. S-70 Main Rotor Characteristics.

Characteristic	English	Metric
Blade number	4	
Nominal rotor RPM	258	
Rotor radius	26.833 ft	8.18 m
Blade chord	20.9 in	53 cm
Rotor solidity	0.0826	
Equivalent blade twist	−18 deg	
Blade tip sweep	20 deg (aft)	
Rotor airfoils	SC1095/SC1095R8	

\

Table 2. Atmospheric Conditions

Condition	English	Metric
Air density	0.002308 slug/ft^3	1.18858 kg/m^3
Air temperature	55.43 °F	13.02 °C
Speed of sound	1112.61 ft/s	339.21 m/s

Model Calibration

One of the challenges of conducting analytical acoustics predictions using compact-chord models with integrated airloads (instead of surface pressures), such as those obtained from a comprehensive analysis code like CAMRAD II, is that blade-vortex interaction noise tends to be over-predicted (Ref. 12). Typically a 6 dB over-prediction is to be expected. Furthermore, these calculations tend to be quite sensitive to the wake model tip vortex core size when the blade-vortex "miss distance" is small. The analytical model employed for the acoustic predictions was therefore calibrated to the measured BVI amplitude from the full-scale UH-60A main rotor wind-tunnel test (Ref. 13) by adjusting the tip vortex core size. The comparison shown in Figure 4 suggests the coupled CAMRAD II/PSU-WOPWOP analytical models adequately captured, or represented, the fundamental governing relationship between BVI noise and aerodynamic angle of attack of the rotor.

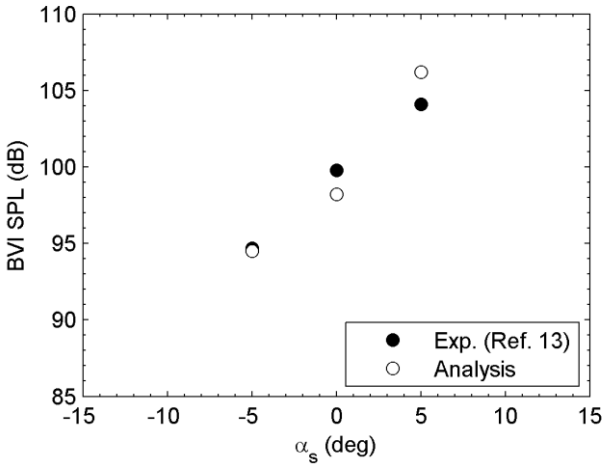

Figure 4. Comparison of acoustic predictions and wind-tunnel BVI measurements (80%-chord core radius)

RESULTS

Rotor Trim

Figure 5 shows the longitudinal rotor blade flapping angle, the shaft tilt (pitch) angle, and the effective rotor tip-path-plane angle of attack for a nominal 6 deg descent case. As the hub pitching moment requirement increases, the rotor tends to flap backwards, becoming zero for zero hub moment trim. As the pitching moment becomes positive, the rotor continues to flap backwards. The solid points represent the trim condition for the free-flight vehicle trim condition reported in Ref. 8.

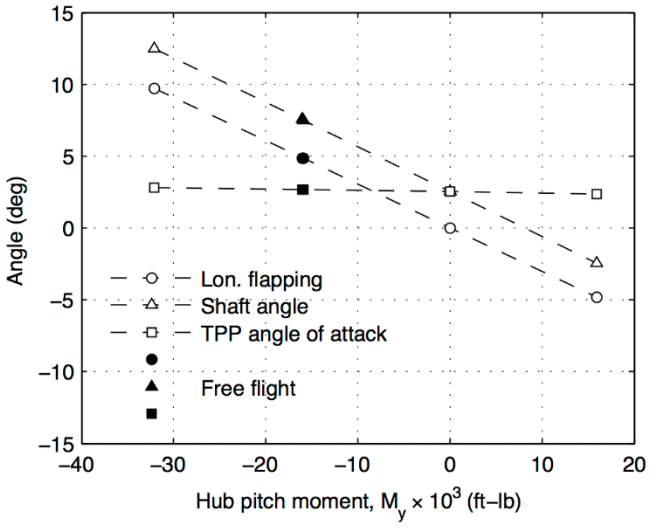

Figure 5. Rotor trim angles for 6 deg descent

Since the rotor thrust and propulsive force requirements were kept constant, the TPP angle of attack remained nearly constant. Figure 5 highlights the non-unique aspect of helicopter trim, i.e., that helicopters can be trimmed to different rotor hub moments for identical flight path trajectories, albeit by allowing the pitch of the vehicle to vary. This is illustrated in Figure 6. In order to ensure the TPP orientation stays constant, however, the shaft angle varies simultaneously at the same rate as the rotor flapping, effectively following the relationship:

$$\alpha_{TPP} = \theta_s - \beta_{1c}$$

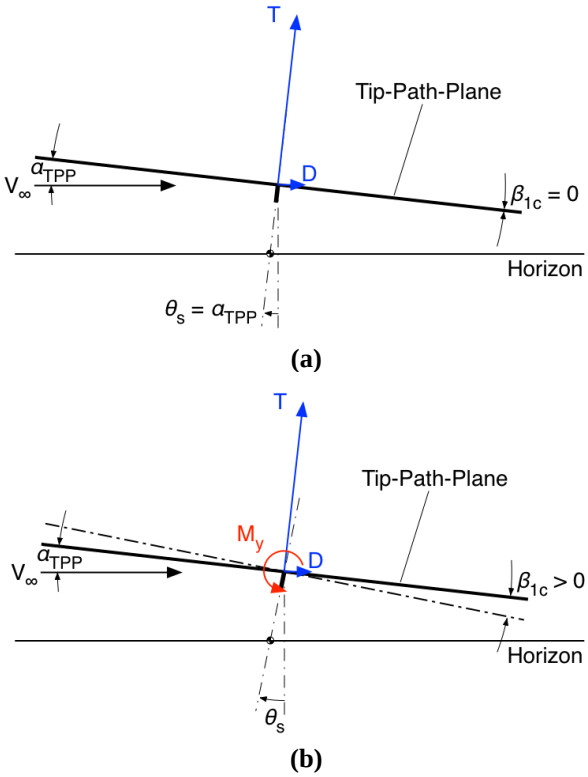

Figure 6. Effect of pitching hub moment on rotor trim: (a) $M_y = 0$, and (b) $M_y < 0$

This trade-off between the shaft angle and the rotor tilt relative to the shaft is further evidenced for the 6 and 12 deg descent conditions shown in Figure 7. The aerodynamic angles of attack for the 6 deg and 12 deg descent angles are 2.7 deg and 8.7 deg, respectively. Of course this would be represented by the constant difference between the shaft angle and longitudinal flapping lines.

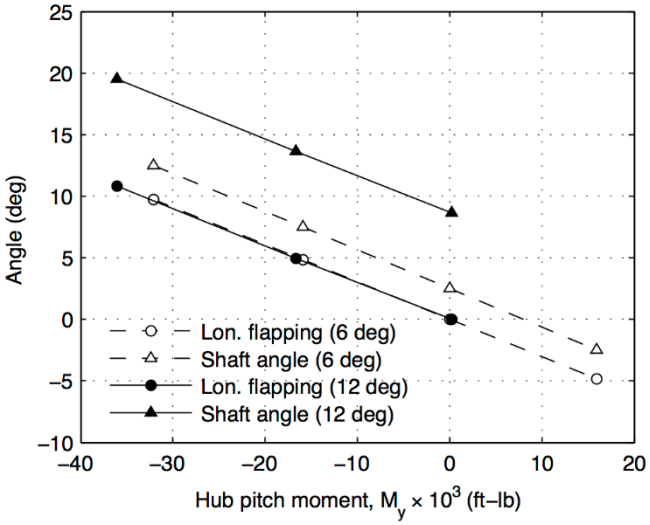

Figure 7. Rotor flapping and shaft angle trade-off

For these particular scenarios, the shaft angle (and rotor flapping) varies nearly 15 deg, overall, between the maximum and minimum values. In practice, there are operational and passenger comfort constraints that require the pilot to operate at desired pitch attitudes. Employing simultaneous control of the vehicle airframe pitching moment, which is necessarily counter-balanced by the hub moment, would enable the use of *X*-force control, where the increase in drag typically causes the vehicle to pitch nose down, while maintaining adequate pitch attitudes.

The rotor hub load limits are a key aspect of using hub pitching moment control. Rotor systems are load limited and for a helicopter of this size, limits of 20,000 to 30,000 ft-lb are typical. Rotors are also limited by the flapping travel (flap stops) which ensures the rotating hub loads stay below endurance limits. These flapping limits typically are on the order of ±7 to ±9 deg. Helicopters can fly above these limits for certain amounts of time based on a usage spectrum. For current rotor technologies, however, the limits shown in the x-axis of Figure 7 probably represent the upper practical limit for this application. The magnitude of the trimmed hub roll moments, shown in Figure 8, is only a small part of the total hub moment. The roll hub moment for the 12-deg configuration is approximately 900 ft-lb. In Figure 7, the roll moments for the 6-deg case are not constant because the trim target was set to satisfy a $\beta_{1s} = 0$ condition (i.e., zero lateral flapping). However, the roll moment remained bounded within ±700 ft-lb margins.

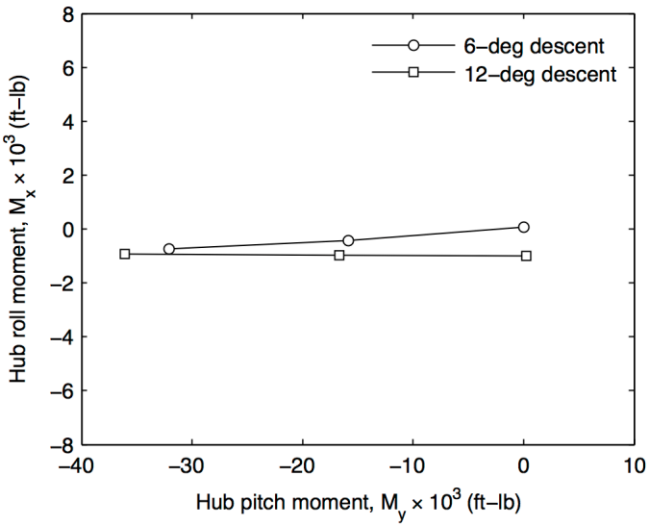

Figure 8. Roll hub moments in trim

Blade-Vortex Interaction Airloads

Little evidence of oblique and parallel BVIs can be found in Figure 9. Analysis of the azimuthal time derivative of the normal force per unit length (in non-dimensional form) distribution over the rotor disk area suggests BVI events are heavily biased towards the blade tip (Figure 9). Additionally, there seems to be a perpendicular BVI around 0.9*R*, which is evident in the forward-advancing side of the rotor (Figure 9(a)).

The location of the BVI events appear to have shifted further aft (earlier) on the advancing side for the steeper descent condition (12 deg), as shown in Figure 9(b). For the 6 deg descent condition, BVIs on the advancing side tended to occur between 45 and 90 deg azimuth, with the largest peak at 68 deg. BVI on the retreating side, after 270 deg azimuth, also occurs. The largest BVI peak in this area occurs in the proximity of 285 deg.

In contrast, the main BVI events for the 12 deg descent case appear for azimuth angles between 29 and 59 deg. Two sharp peaks at 29 and 39 deg are evident in Figure 10(c), which shows a comparison of the airload derivatives at a blade span of 0.92*R*. Two smaller peaks appear near 49 deg and 59 deg.

Figure 10 shows that, except for the weaker interaction near 60 deg, the differences between the airload derivatives for the three hub moments are negligible. The oscillation observed between 90 and 180 deg azimuth for the 0 ft-lb case is not expected to be a significant source of noise at the BVI frequencies. This result suggests that BVI noise differences between the three cases may not be acoustically significant.

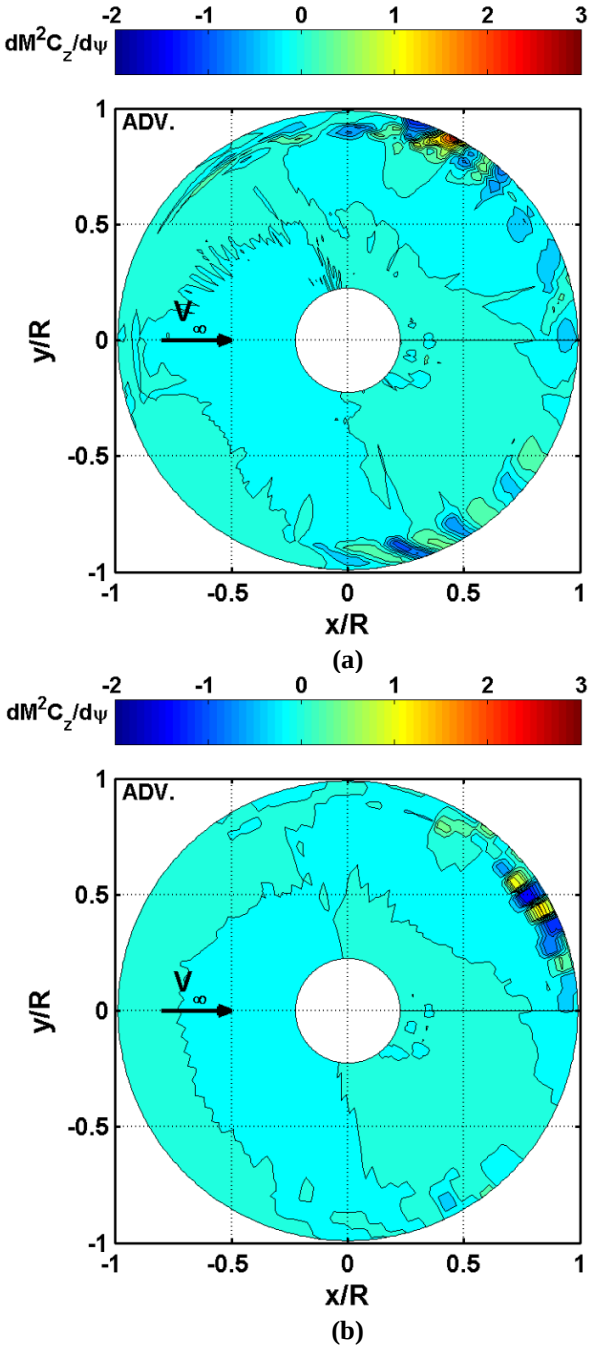

Figure 9. Azimuthal time derivative of the normal sectional force: (a) 6 deg baseline ($M_y \approx -16{,}000$ ft-lb), and (b) 12 deg baseline ($M_y \approx -16{,}600$ ft-lb)

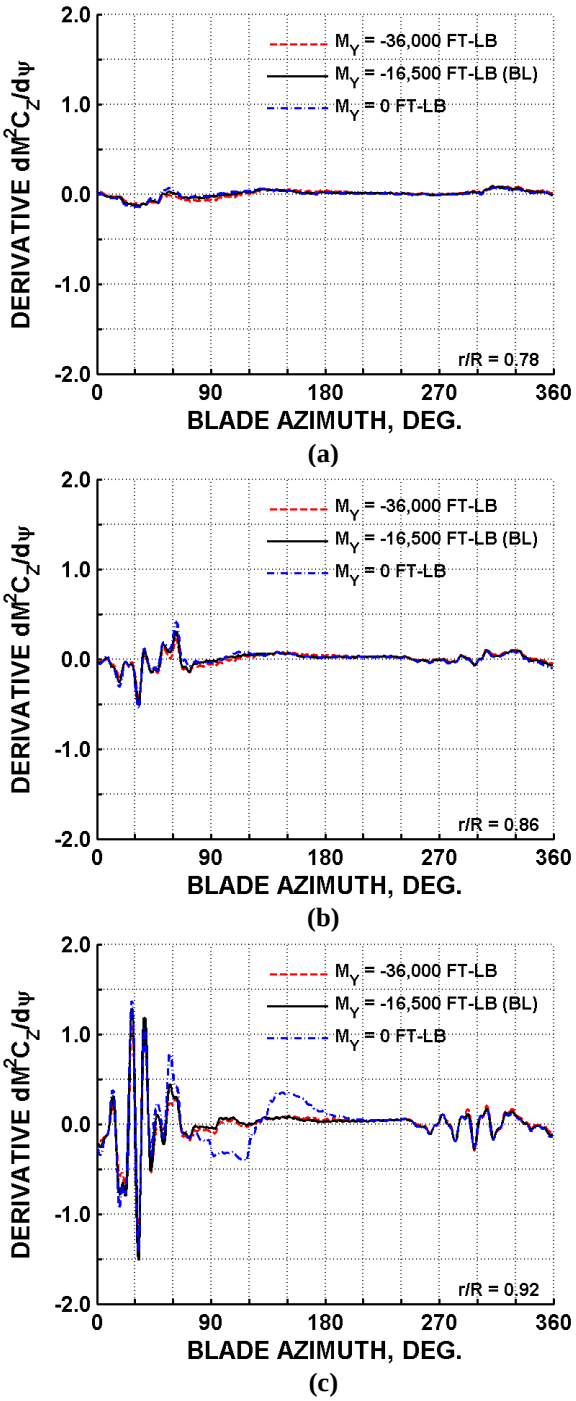

Figure 10. Comparison of normal force per unit span derivatives for various hub moments (12 deg descent)

Blade Motion

The TPP orientation for all three cases (for a given descent angle) stayed approximately constant (satisfying lift and propulsive force equilibrium). The blade tip was observed, however, to undergo a higher harmonic oscillations (2/rev and higher) of varying amplitudes for each case (Figure 11). This 2/rev oscillation could be causing the blade-vortex miss distance to vary slightly for each case. The variation in the blade position at an azimuth of 54 deg, for example, is shown in Figure 12. The higher negative hub moment (M_y = −36,000 ft-lb) was shown to force the blade down, further away from the TPP. The positive moment had the opposite effect.

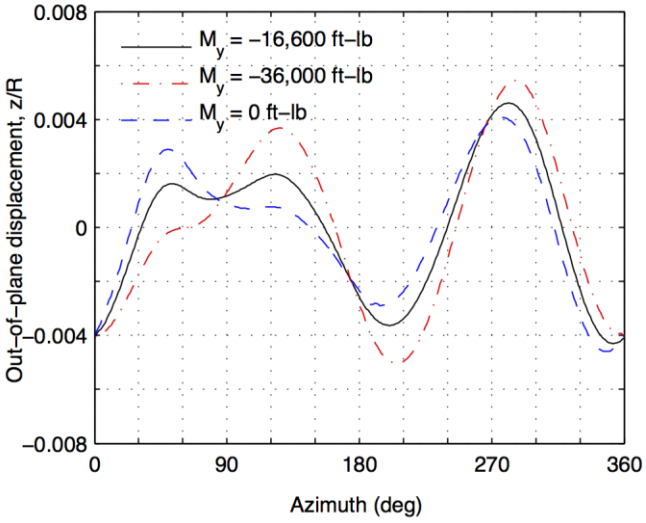

Figure 11. Tip motion relative to the TPP

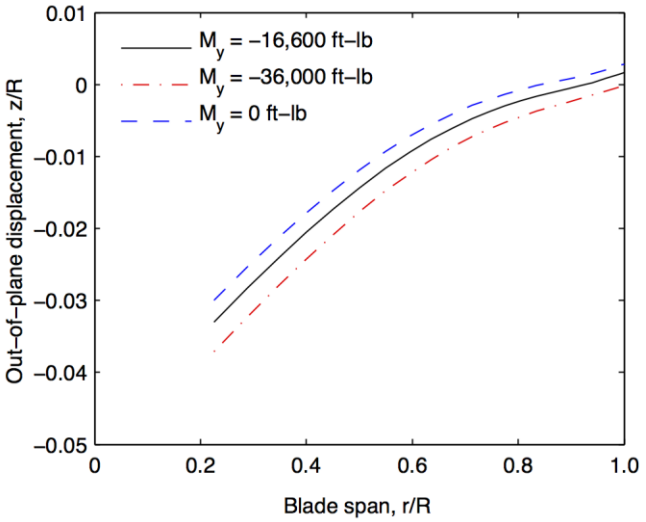

Figure 12. Elastic blade deformation in the TPP frame of reference (z = 0 defines the TPP)

Miss Distances

The contours shown in Figure 13 represent the absolute distance between the blade and the nearest vortex filament, i.e., the length of the shortest line that can be drawn between a point on the blade and a point on the nearest tip vortex. Defined in this fashion, the miss distance metric is always positive, reaching a value equal to zero only where there is a direct impact. For the descent condition shown (12 deg), however, the wake was found to be above the rotor plane. As expected, the normal force derivative peaks shown in Figure 10(c) roughly corresponded to the instances where the miss distance approximated zero (the local minima in Figure 13).

The differences in miss distance (relative to the baseline case of 12 deg descent and M_y = −16,600 ft-lb), shown in Figure 14, better illustrate the effect of the pitching moment. The hub moment M_y = −36,000 ft-lb caused the miss

distance at the 54 deg azimuthal location to increase (see Figure 14(a)). This result is consistent with the elastic blade deformation from Figure 12. Accordingly, the miss distance for M_y = 0 ft-lb (Figure 14(b)) decreased at this azimuth (54 deg). These variations in the miss distance are likely the cause of the variations in the peaks of the normal force derivative (Figure 10(c)) at this azimuth.

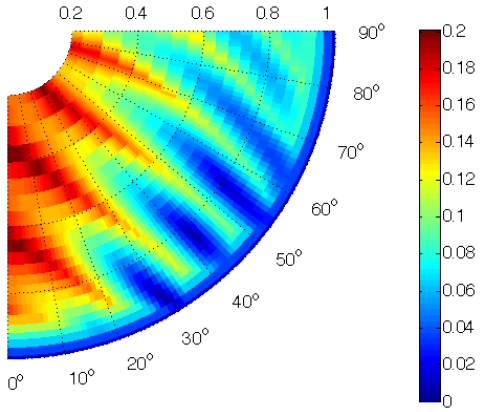

Figure 13. Rotor-wake miss distance in rotor radii (12 deg descent condition, $M_y \approx -16{,}600$ ft-lb)

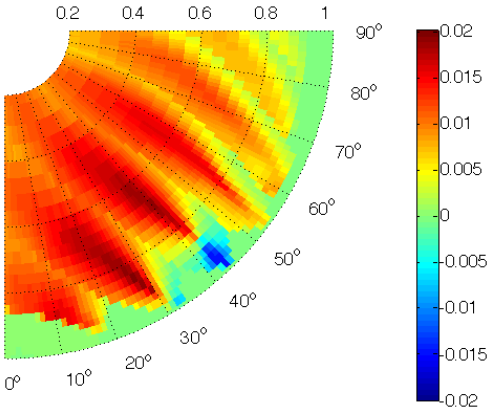

(a)

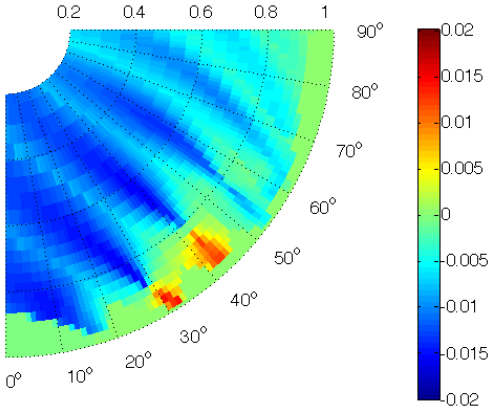

(b)

Figure 14. Rotor-wake miss distance in rotor radii, differences relative to baseline (12 deg descent condition, $M_y \approx -16{,}600$ ft-lb) for: (a) $M_y \approx -36{,}000$ ft-lb, and (b) $M_y \approx 0$ ft-lb

The decrease, or increase, of the miss distance shown in Figure 14, in response to the change in hub moment, was not uniform thorughout the blade rotation. Opposite effects ocurred at 29 and 42 deg. These results suggest that while the main BVI event occuring at 55 deg was attenuated for a negative pitch hub moment change, this attenuation was negated by the strengthening of the BVI event at 42 deg. The opposite trade-off occurs for a positive hub moment change, but in both instances the potential net BVI noise reduction is cancelled.

Baseline BVI Sound Pressure Level (BVI SPL)

The effect of the change in the tip-path-plane angle of attack (α_{TPP}) on the BVI SPL is illustrated in Figure 15. Recall that the angles of attack for the 6 deg and 12 deg descents are 2.7 and 8.7 deg, respectively. The BVI SPL (in dB) was computed for a hemispherical grid of observers (indicated by the white markers) located 500 ft from the rotor hub center. The differences in the radiated noise at this distance, for the two descent conditions, are evident in: 1) the directivity, and 2) the magnitude changes of the BVI SPL hotspot. For the steeper 12 deg descent condition, the hotspot migrated approximately 40 deg aft (earlier), from an azimuth of 160 deg for the 6 deg case, to approximately 120 deg. This change is because as the tip-path-plane angle of attack increases, the miss distance associated with interactions near the front of the rotor disk tend to increase, while those closer to the rear of the rotor tend to decrease. Figure 16 plots the difference between the miss distances for the 12 deg descent condition relative to the 6 deg descent. The steeper descent caused the miss distances to decrease for the outboard stations near the rear of the rotor disk, but increase for blade azimuths closer to the front of the rotor disk. The BVI closer to the rear of the advancing side of the rotor disk radiate noise more towards the advancing side than those closer to the front.

The region of BVI SPL exceeding 93 dB is shown in Figure 15 to have expanded significantly for the 12 deg descent condition, relative to the 6 deg case. The peak BVI SPL for the 12 deg condition was approximately 94.8 dB. This represented only a moderate increase over the 93.2 dB BVI SPL calculated for the 6 deg descent condition.

Judging by the position of the wake, which is below the rotor for the 6 deg descent condition and above the rotor for the 12 deg descent case, the analysis likely missed capturing the maximum BVI condition for this helicopter configuration. The descent condition for minimizing miss distance near the parallel interaction around 55 deg blade azimuth, and resulting in the maximum BVI SPL, is probably near 9 deg, but unfortunately the free wake methods employed in the comprehensive analysis failed to converge in this regime.

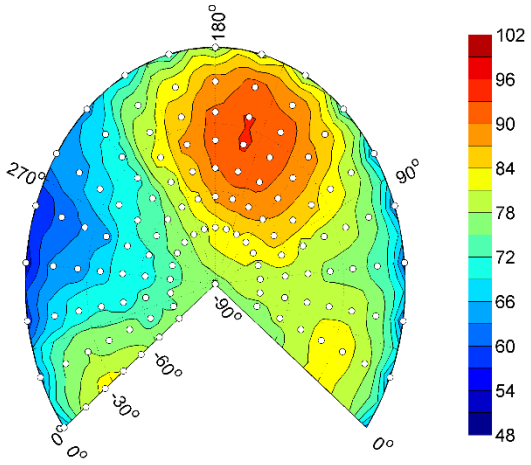

(a)

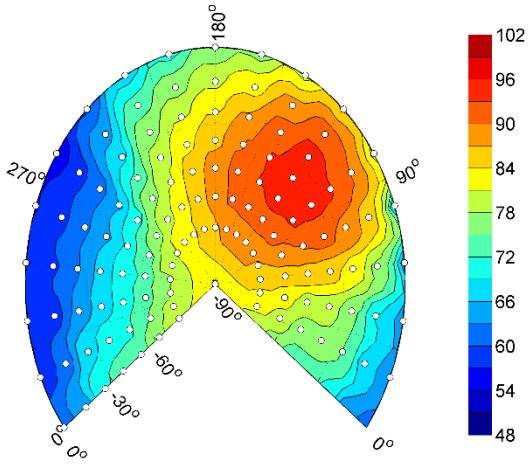

(b)

Figure 15. BVI SPL (dB) baseline contours for: (a) 6 deg ($M_y \approx -16{,}000$ ft-lb), and (b) 12 deg ($M_y \approx -16{,}600$ ft-lb)

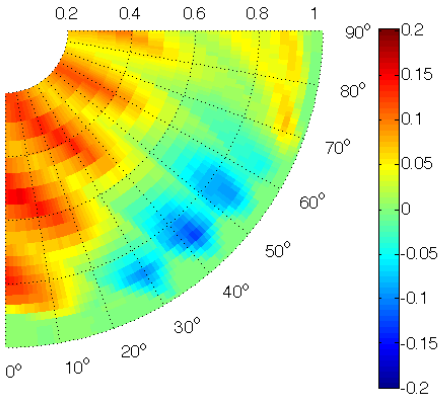

Figure 16. Change in rotor-wake miss distance in rotor radii between baseline 12 and 6 deg descent conditions.

Effect of Hub Moment Trim on BVI SPL

The peak BVI SPL for the configurations that were analyzed was found to be insensitive to changes in the hub pitching moment (Figure 17). The largest reduction, relative to the baseline was 1 dB. This reduction was achieved with a negative pitching moment on the order of −36,000 ft-lb. More significant reductions may be achieved for larger pitching moments, but these moments exceed the limits of the S-70 rotor system.

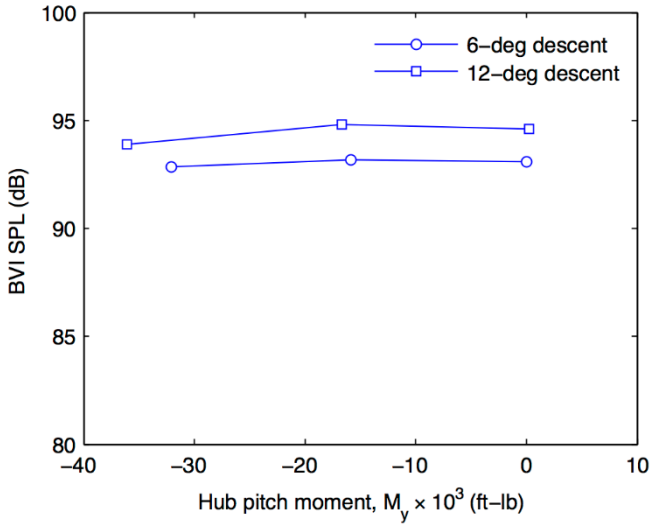

Figure 17. Peak BVI SPL

The acoustic pressures for an observer near the peak BVI SPL condition (120 deg azimuth, 40 deg elevation) for the 12 deg descent case are shown in Figure 18. Only one-quarter of a revolution is shown. At this microphone location, there are little or no contributions from thickness monopole. Acoustics time histories are dominated by the impulsive fluctuations associated with BVI. Note that these time histories have been filtered to reflect only energies between 10th and 50th blade passage harmonics. A slight change in the amplitude of the peak-to-peak acoustic pressure was predicted with varying hub pitch moments.

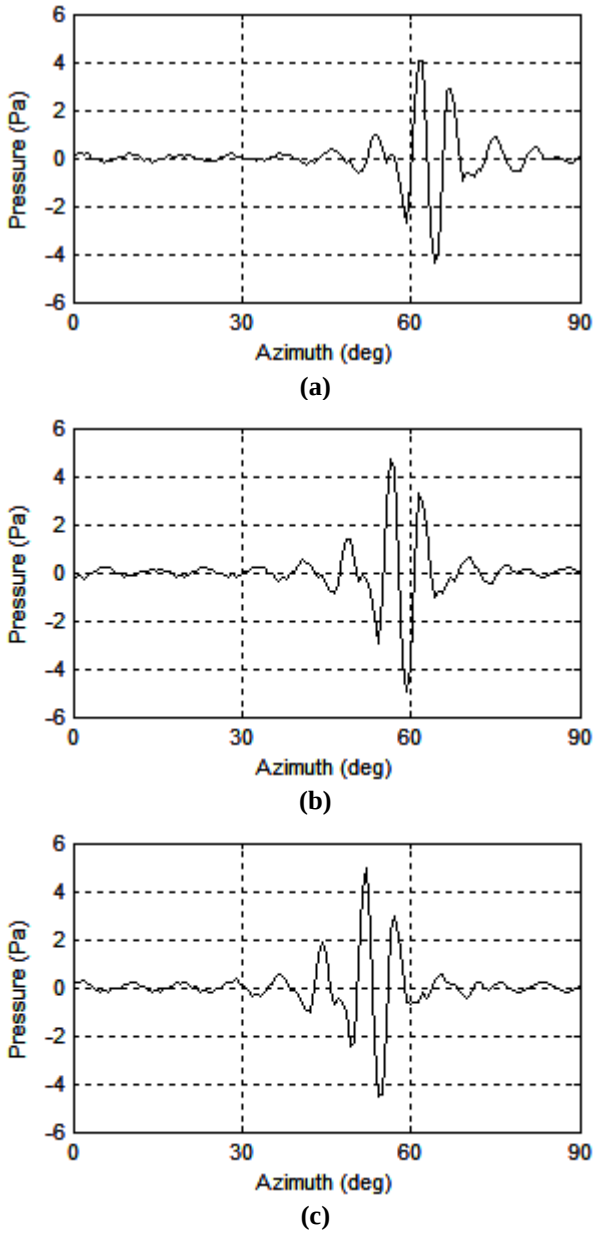

Figure 18. Acoustic pressures near peak BVI SPL for: (a) $M_y \approx -36{,}000$, (b) $M_y \approx -16{,}600$ and (b) $M_y \approx 0$ ft-lb (12 deg descent)

Figures 19-22 summarize the BVI Sound Pressure Level (SPL) calculations for the four non-baseline cases. Again, results were computed for a 500-ft hemispherical observer grid located below the rotor. Baseline BVI SPL calculations (Figure 15) are shown again for clarity. Figures 19 and 20 illustrate the effect of a negative change of the hub pitch moment for the two descent conditions. Figures 21 and 22 illustrate the effect of a positive change of the hub moment. There is a small but noticeable reduction of the BVI hotspot in Figure 20. Overall, however, these results primarily highlight the relative insensitivity of the BVI noise to the four parametric hub moment variations.

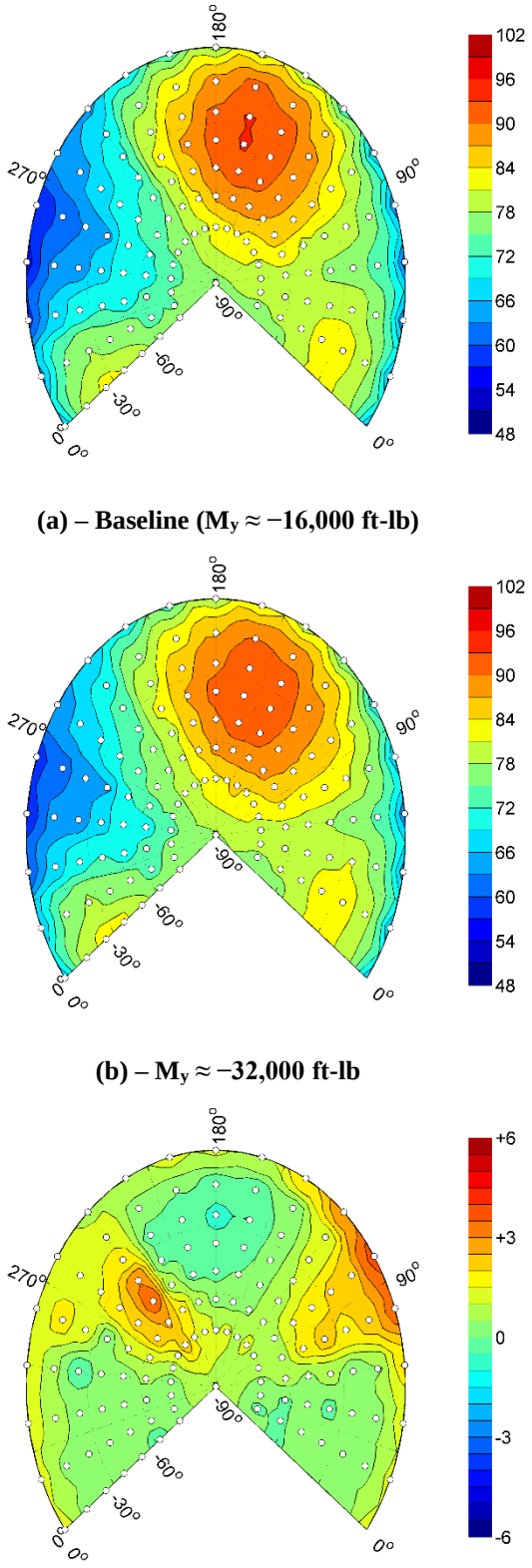

(a) – Baseline ($M_y \approx -16{,}000$ ft-lb)

(b) – $M_y \approx -32{,}000$ ft-lb

(c) – Difference

Figure 19. BVI SPL (dB) difference for a negative trim pitch hub moment variation (6 deg descent)

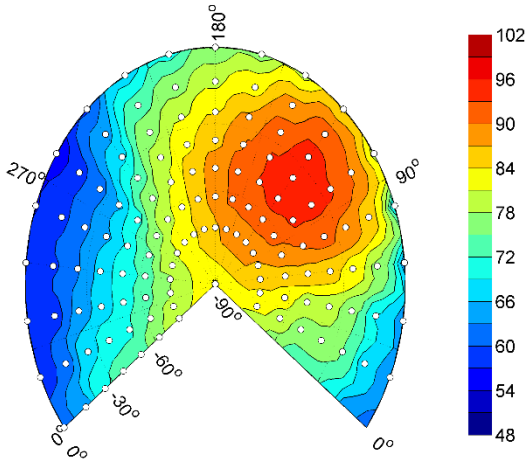

(a) – Baseline ($M_y \approx -16{,}600$ ft-lb)

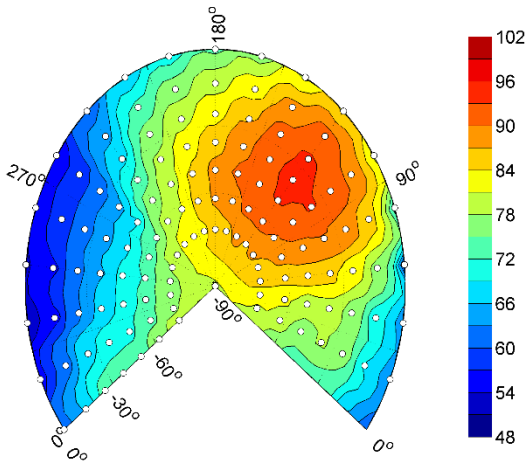

(b) – $M_y \approx -36{,}000$ ft-lb

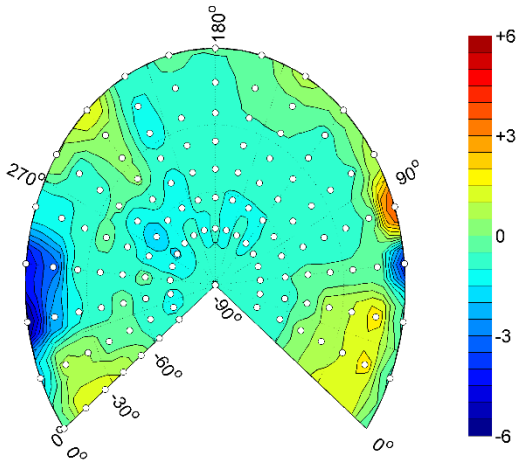

(c) – Difference

Figure 20. BVI SPL (dB) difference for a negative trim pitch hub moment variation (12 deg descent)

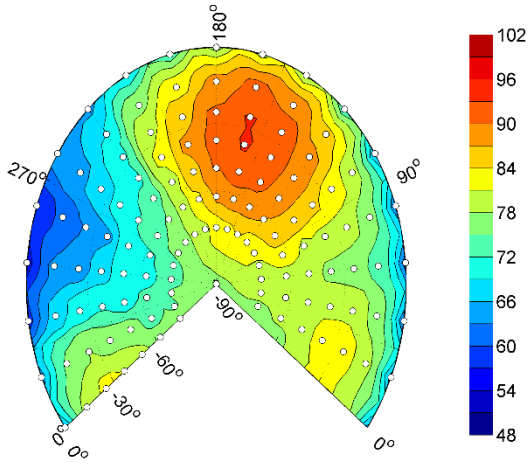

(a) – Baseline ($M_y \approx -16{,}000$ ft-lb)

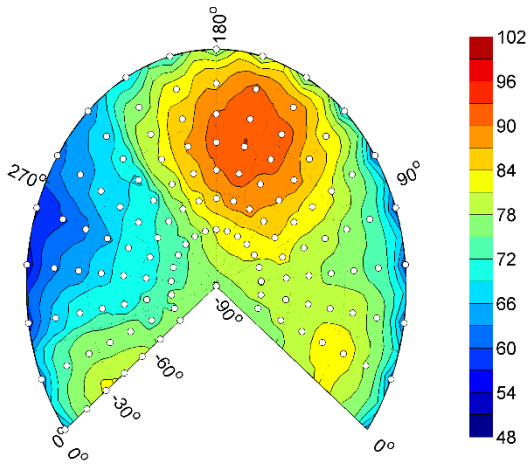

(b) – $M_y \approx 0$ ft-lb

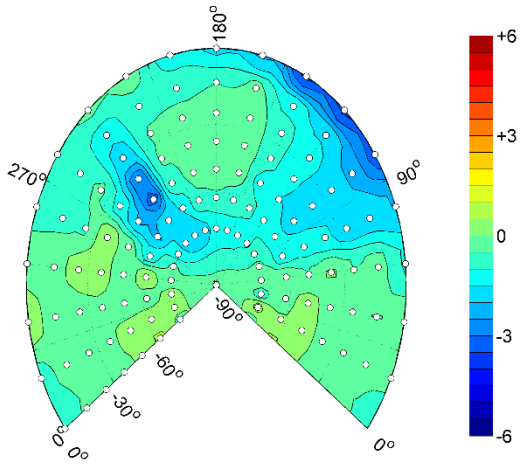

(c) – Difference

Figure 21. BVI SPL (dB) difference for a positive trim pitch hub moment variation (6 deg descent)

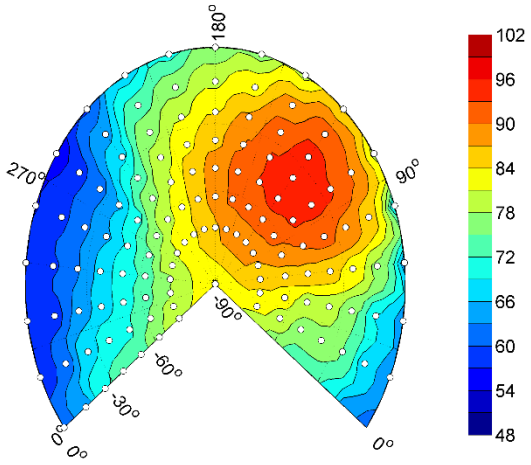

(a) – Baseline ($M_y \approx -16{,}600$ ft-lb)

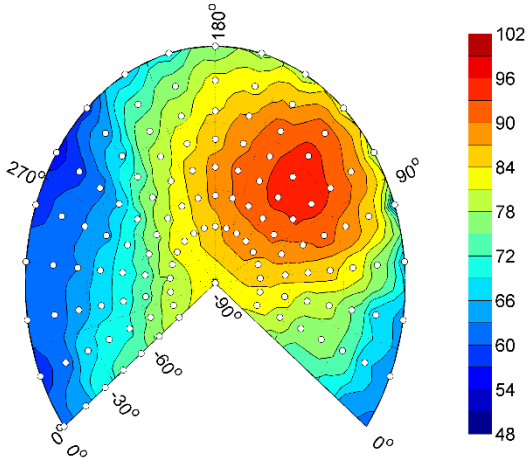

(b) – $M_y \approx 0$ ft-lb

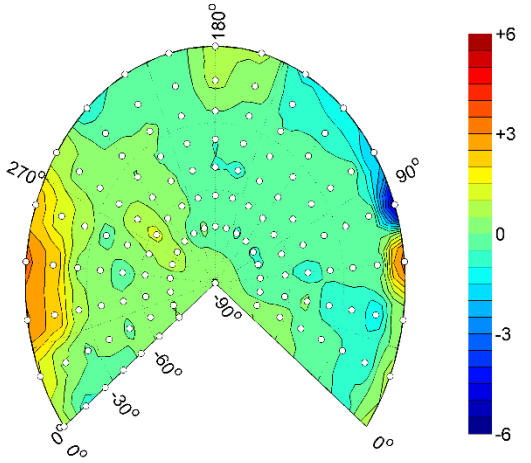

(c) – Difference

Figure 22. BVI SPL (dB) difference for a positive trim pitch hub moment variation (12 deg descent)

DISCUSSION

While the results of this analysis suggest the overall effect of changing hub pitching moment on the BVI noise radiated by the main rotor is small, there are several aspects of this work worth discussing.

Results from the comprehensive and acoustic analyses imply how the wake and blade motions have responded to the additional pitching moment. The phase and amplitude changes of the 2/rev (and higher) elastic flapping of the blade could magnify or reduce the miss distance of the dominant BVI event. Negative changes in the pitching moment caused the miss distance to increase, weakening the BVI event. Positive changes in the pitching moment had the opposite effect. However, these changes also had effects on secondary BVI events, either magnifying or reducing them. Such effects were found to often mitigate the impact of the dominant BVI event.

Fuselage Attitude Control

One of the primary motivations for this study was to investigate the effect of pitching moment in the context of fuselage attitude control in conjunction with concepts such as *X*-force control. The application of a drag force on the fuselage, as is the basic principle of *X*-force control, to reduce BVI noise by inducing changes in the tip-path-plane angle has been well documented. Without a means of controlling the pitching moment, such concepts result in large changes of the fuselage pitch. The acoustics results presented in this paper suggest that pitching moments could be applied to regulate the attitude of the fuselage without incurring BVI acoustic penalties.

Hub Moment Limits

The parametric values of the hub moment that were chosen for this analysis were selected to be representative of the actual limits of the helicopter rotor studied. Although the effect of pitching moment on BVI noise was small (1 dB) for the range of hub moments studied in this paper, pitching moment was shown to have some effect on blade-vortex miss distance. Application of larger hub pitching moments is likely to cause more significant changes in BVI noise.

Aerodynamic devices applying large pitching moments (and therefore large hub moments in trimmed flight) are not without precedent. For example, the Sikorsky S-67 Blackhawk helicopter, shown in Figure 23, featured a set of dive brakes located on a low wing well below the helicopter fuselage center of gravity. Application of these brakes caused an increase in the effective flat plate drag area of the helicopter by 37 ft^2 at 140 knots, resulting in an estimated nose-down pitching moment on the order of 70,000 ft-lb during cruising flight conditions. These brakes were used to apply *X*-force for rapid deceleration and to pitch down and stabilize the fuselage attitude to facilitate weapons employment during strafing (Ref. 14). Later, the NASA/Army Rotor Systems Research Aircraft (RSRA)—derived from the S-67—would be specifically designed to allow the rotor to counter-hold a 75,000 ft-lb pitching moment applied by full-down deflection of wing-mounted

flaps at 120 knots airspeed (Ref. 15). This aircraft is pictured in Figure 24.

Figure 23. Sikorsky S-67 Blackhawk with drag brakes fully deployed (Source: US Army).

Figure 24. RSRA in compound helicopter configuration (Source: NASA).

Comprehensive Analysis Limitations

As with any rotorcraft acoustic analysis, the limitations typically are not the acoustics prediction, but the ability to accurately calculate the rotor aerodynamic forces. In this case the lifting-line BVI model may be particularly limiting.

Firstly, the tip vortex model was initially calibrated in order to match wind-tunnel acoustic measurements, resulting in a tip vortex core radius equal to 80% of the chord length. Therefore, the BVI acoustic pressures may be insensitive to the changes in miss distance since the distances are of the same order as the vortex core size. Hypothetically, one could shrink the core size, and likely see a bigger effect on noise.

Secondly, reducing the vortex core size also has implications for the convergence of the model. At 80% of the chord length, the inflow model had difficulties converging, preventing the rotor to trim between 9 and 12 deg descent conditions, where maximum BVI would be expected. Every attempt to push the wake into the rotor, such as reducing thrust or drag, resulted in these same convergence problems. This issue should be investigated further using CFD methodologies, which may better reflect the physics of BVI when miss distances are small.

CONCLUSIONS

Results from the comprehensive analysis and acoustics predictions lead to the following conclusions:

1. Varying the rotor hub pitching moment caused small changes in the wake and blade motions, which led to increases or decreases of the miss distance by nearly 0.5 ft.

2. Varying the fuselage pitching moment caused small changes in the peak BVI noise radiated. These BVI noise changes are the result of small variations in the miss distance of the dominant BVI.

3. Reductions or increases in the miss distance were not uniform around the blade azimuth. Changes in the miss distance of the dominant BVI event were accompanied by opposite changes of secondary BVI events.

4. Application of rotor hub pitching moment can be used to control the rotor shaft angle, and therefore fuselage pitch attitude, during trimmed flight. Changes in rotor shaft angle of ±6 degrees were possible within the hub moment limits of the S-70 rotor system. This could be used to compensate for the uncomfortable change in fuselage pitch attitude introduced by a fuselage-mounted *X*-force BVI noise controller.

REFERENCES

[1]Schmitz, F. H., "Rotor Noise," *Aeroacoustics of Flight Vehicles, Theory and Practice, Vol. 1: Noise Sources*, Ch. 2., Published for the Acoustical Society of America through the American Institute of Physics, 1995.

[2]Leverton, J. W., "Helicopter Noise: What is the Problem?," *VERTIFLITE*, Vol. 60, No. 2, March/April 2014, pp. 12-15.

[3]Jacklin, S. A. et al., "Full-Scale Wind Tunnel Test of an Individual Blade Control System for a UH-60 Helicopter," American Helicopter Society 58th Annual Forum, Montreal, Canada, June 11-13, 2002.

[4]Sim, B. W., JanakiRam, R. D., and Lau, B. H., "Reduced In-Plane, Low Frequency Noise of an Active Flap Rotor," American Helicopter Society 65th Annual Forum, Grapevine, TX, May 27-29, 2009.

[5]Schmitz, F. H., "Reduction of Blade-Vortex Interaction (BVI) Noise Through X-Force Control," NASA TM-110371, September 1995.

[6]Schmitz, F. H., Gopalan, G., and Sim, B. WC., "Flight-Path Management/Control Methodology to Reduce Helicopter Blade–Vortex Interaction Noise," *Journal of Aircraft*, Vol. 39, (2), March-April 2002, pp. 193-205.

[7]Conner, D. A., Edwards, B. D., Decker, W. A., Marcolini, M. A., and Klein, P. D., "NASA/Army/Bell XV-15 Tiltrotor Low Noise Terminal Area Operations Flight Research Program," *Journal of the American Helicopter Society*, Vol. 47, (4), October 2002, pp. 219-232.

[8]Malpica, C., Greenwood, E., and Sim, B., "Helicopter Non-Unique Trim Strategies for Blade-Vortex Interaction (BVI) Noise Reduction," Presented at the AHS Technical Meeting on Aeromechanics Design for Vertical Lift, San Francisco, CA, January 20-22, 2016.

[9]Johnson, W., "Rotorcraft Aerodynamics Models for a Comprehensive Analysis," American Helicopter Society 54th Annual Forum, Washington, DC, May 20-22, 1998.

[10]Shirey, J. S., Brentner, K. S., and Chen, Hn., "A Validation Study of the PSU-WOPWOP Rotor Noise Prediction System," 45th AIAA Aerospace Sciences Meeting and Exhibit, Reno, NV, January 8-11, 2007.

[11]Farassat, F., "Derivation of Formulations 1 and 1A of Farassat," NASA/TM-2007-214853, March 2007.

[12]Sim, B. WC. and Schmitz, F. H., "Blade-Vortex Interaction (BVI) Noise: Retreating Side Characteristics," Proceedings of the American Helicopter Society (AHS) Aeromechanics Specialists' Meeting, Atlanta, GA, November 13-14, 2000.

[13]Kitaplioglu, C., "Aeroacoustic Test of a Full-Scale UH-60 Main Rotor in the NASA Ames 80- by 120-Foot Wind Tunnel," NASA/TM - 2006 - 213487, August 2006.

[14]Yamakawa, G. M. et al., "Attack Helicopter Evaluation, Blackhawk S-67 Helicopter, Final Report," AVSCOM AD-771 161, July 1972.

[15]Schmidt, S. A. and Linden, A. W., "Rotor Systems Research Aircraft Predesign Study," NASA/CR-112154, October 1972.